Wave buoys in current – experimental results and observations

Samuel Draycott, Ajit C Pillai, Roman Gabl, and Thomas Davey

Abstract—**Wave buoys are used extensively for the characterisation of deployment locations for offshore technologies, where they are subjected to currents in addition to the ocean waves. It has been frequently observed that the measurements from wave buoys are affected by these currents, but the majority of deployed buoys cannot measure, or account for, this effect. Presented here are a series of experiments conducted at the FloWave Ocean Energy Research Facility, deploying a spherical wave buoy scale model with a simplified mooring in a series of combined wave-current sea states. The resulting open-access dataset provides 6 degree of freedom buoy motion and force data (current only) in addition to wave gauge and acoustic doppler velocimeter measurements of the sea states. Experiments were conducted under a range of combined wave-current conditions with variables including velocity, wave period, and relative wave-current angle. It is observed that vortex induced motions (VIM) are significant and highly sensitive to the mooring configuration and current speed. Nevertheless, the wave-induced response and buoy motion amplitude is found to agree with linear wave-current theory predictions in most following wave-current conditions. This agreement is poorer in opposing conditions where larger surge motions than predicted are consistently observed. Wave buoy outputs in directional irregular seas were also found to closely match wave gauge outputs.**

If properly considered, it is suggested that the effect of the current on existing buoy technologies may be accounted for without hardware modification or additional sensing, but through updated analytical tools.

Index Terms—**Wave buoys, Experimental testing, Wave-current interaction, Vortex-induced motions, Directional waves**

I. Introduction

WAVE buoys are the most widely used device for the measurement of ocean waves [1] and are commonly used to define operational and extreme conditions for the design of offshore systems and devices. They are often used to calibrate and validate wide-area numerical models to gain an understanding of the wave climate over larger areas and/or time-frames. The presence of an unknown current, however, will introduce errors into estimated sea state parameters which will diminish the accuracy of numerical models and the reliability of the design process.

It is well known that buoy measurements are affected by the presence of currents [2]–[4], yet only recently have buoys been developed which can measure both waves and currents (e.g. [5], [6]). Errors arise in estimated sea state parameters, when operating in the presence of an unknown current, due to: (i) a modification to the dispersion relation which is not considered or known during processing; and, (ii) modification to the buoys dynamic response due to alterations to the mooring line tension and draught introduced from current-induced drag. The total errors result from a combination of the (usually unknown) altered resource and the buoys response to it.

As is discussed further in Section II, an unknown current will introduce errors in the assumed wavelengths, steepness and power. For wave energy converters (WECs), this may result in sub-optimal design, tuning and control of the system with the potential for reduced power output and insufficient design for extreme conditions. The unknown current will also introduce a drag force on the system which will affect the mooring tensions, subsequent dynamics and interaction with the WEC. Hence, the current is important to understand and quantify, yet is routinely ignored in buoy processing and site characterisation.

To address this, the Supergen ORE Hub Flexible Fund *Accounting for current in wave buoy measurements* project aims to develop a robust method for processing wave buoy data in the presence of current. Towards this aim, a framework was developed in [7] to account for the presence of current in wave buoy processing; correcting sea state parameters and providing an estimate of the current velocity. In [7], the framework developed is based on a parameter estimation optimisation approach where the error between measured and theoretical cross-spectra is minimised. To generate theoretical cross-spectra, the buoy is assumed to track the current modified waves perfectly and any modified dynamics were omitted during preliminary validation. The aim of the present paper is, therefore, to assess modified buoy dynamics in the presence of current. This is achieved through scaled experiments carried out in the FloWave combined wave-current facility – enabling the generation of waves and currents at arbitrary angles. Forces and buoy displacements are measured in wave-only, current-only, and combined wave-current conditions. Regular waves, including oblique cases, are presented along with example outputs for directionally spread irregular conditions.

This work was funded by the EPSRC-funded SuperGen Offshore Renewable Energy Hub (grant no: EP/S000747/1) under the "Accounting for Currents in Wave Buoy Measurements" project

Samuel Draycott is with the Department of Mechanical, Aerospace and Civil Engineering, School of Engineering, University of Manchester, UK (e-mail: Samuel.Draycott@manchester.ac.uk).

Ajit C Pillai is with the Renewable Energy Group, College of Engineering, Mathematics and Physical Sciences, University of Exeter (e-mail: A.Pillai@exeter.ac.uk)

Roman Gabl is with the FloWave Ocean Energy Research Facility, School of Engineering, University of Edinburgh (e-mail: Roman.Gabl@ed.ac.uk)

Thomas Davey is with the FloWave Ocean Energy Research Facility, School of Engineering, University of Edinburgh (e-mail: Tom.Davey@FloWave.ed.ac.uk)

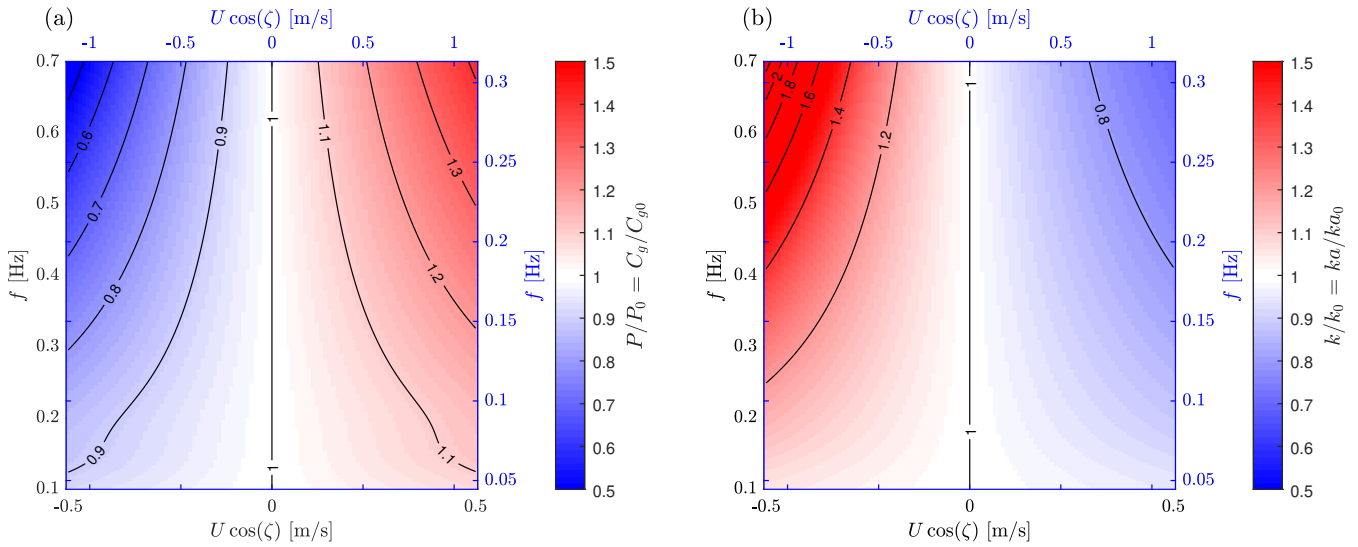

Fig. 1. Relative errors in (a) sea state power and group velocity, and (b) sea state steepness and wavenumber, if current is ignored (subscript 0) for a range of frequency and relative current velocities. Tank-scale values of frequency and relative current velocities are shown on black axes (bottom and left), whilst representative full-scale values (assuming 1:5 scale based on tank scale depth of 2 m and full-scale depth of 10 m) are shown on the blue axes (top and right). Note that $P/P_0 = C_g/C_{g0}$ and $k/k_0 = ka/ka_0$ as the wave amplitudes, a, are assumed to be accurately measured by the buoy in the presence of current.

These experiments provide a benchmark dataset to develop fundamental understanding and validate hydrodynamic models. Validated hydrodynamic models can subsequently be used to expand the understanding gained to full-scale buoys with varied geometries and mooring configurations which can be incorporated into buoy processing methodologies such as the methodology developed by the authors in [7] (through transfer functions).

This paper is laid out as follows: Section II outlines in more detail the sources of the errors introduced by the presence of a current. Section III describes the experimental methodology including the model design & manufacture, experimental set-up and test plan. Results are presented in Section IV. A discussion on expanding and extrapolating the understanding to full-scale buoys is presented in Section V, with concluding remarks offered in Section VI.

II. Errors Introduced as a Result of Current

When there is an unknown current there are different types of errors which will arise when processing wave buoy data. As mentioned above, these are fundamentally associated with the modified wave climate and the modified buoy response. In terms of the underlying wave climate, current introduces a Doppler shift which modifies the wavenumbers associated with frequencies observed in the buoy's reference frame. Wave heights will also be modified, yet these should be measured relatively accurately by the buoy. The modified dispersion relation, accounting for the presence of a current is [8]:

$$\omega - kU\cos\zeta = \omega_r = \sqrt{gk\tanh kd} \tag{1}$$

where k is the wavenumber, ω is the angular frequency in the fixed reference frame (observed by the buoy), d is the water depth and g is the acceleration due to gravity. U is the current speed and ζ is the relative angle between the wave and current fields, where $\zeta = 0$ for waves travelling on a following current. ω_r is the angular frequency observed in a reference frame moving with the steady current.

The group velocity, C_g, can be expressed as:

$$C_g = \frac{C}{2}\left(1 + \frac{2kh}{\sinh(2kh)}\right) \tag{2}$$

where $C = \omega/k$ is the phase speed in the fixed reference frame.

Noting that sea state steepness $s \propto k$ and power $P \propto C_g$, if U is assumed to be zero there will be errors in both of these parameters for the range of wave frequencies measured by the buoy (from the z measurements). The expected errors observed in $P(C_g)$ and $s(k)$ are presented in Fig. 1 a) and b) respectively. Tank-scale (FloWave) conditions and the associated errors are presented, along with representative full-scale combinations. The representative full-scale equivalents on Fig. 1 are calculated at 1:5 scale, which assumes a relatively small full-scale wave buoy diameter and water depth. Large errors are expected for high-frequency wave conditions in appreciable currents, where the group velocities are lowest and, hence, the effect of current the largest. It is interesting to note that, over a theoretical rectilinear tidal cycle, the mean power will be unaffected by current, yet the mean wavenumbers (wavelengths) and steepness will be biased towards the values associated with the opposing current. Hence, tuning wave energy converter response/configuration for the dominant wavelengths present at a site would be sub-optimal without proper appreciation of the current. In addition, extremes extrapolated from data and used to define design load cases will ignore the effect of the current itself and the associated modified wavenumbers, and hence simulated kinematics may not be representative of the true extreme events and could lead to under-design.

In addition to the modified wave climate, the current will also affect the buoy response to the modified waves. The current-induced drag will introduce tension into the mooring line and an alteration to the buoy draught (for many mooring configurations). This will alter the buoys response and result in unknown transfer functions, $H_n(f, \theta, U)$, which relate the buoys motions (n = 1→3) to the underlying surface elevation. Most modern buoys are z-x-y displacement buoys, and hence n = 1, 2, 3 corresponds to z, x and y motions respectively. The heave (z) spectrum is used to define the non-directional frequency spectrum, whilst a combination of the three measurements provides estimates of directional parameters (see e.g. [9]).

If the buoy was still able to perfectly capture the underlying surface, based on linear wave theory, $H_n(f, \theta, U)$ for an z-x-y buoy would correspond to:

$$H(f, \theta, U) = \left[1, \frac{\cos(\theta)}{\tanh(kd)}, \frac{\sin(\theta)}{\tanh(kd)}\right] \tag{3}$$

noting that in current, the calculated wavenumbers, k associated with frequency, f, must consider the Doppler shift as per Eq. (1) and hence, for a given frequency, are a function of the current speed and relative direction. θ is the wave direction relative to the x-axis. Using standard buoy processing methodologies and assumptions, an incorrect relationship between the buoy motions and the true surface would be assumed (incorrect k, independent of current and direction), resulting in errors in sea state directionality. If the buoy motions can be modelled using Eq. (3), then it has recently been shown to be possible to predict the wavenumbers and current velocity (and hence correct sea state parameters) from the modifications to the x and y motions at the observation frequencies – even for complex directionally spread seas [7]. In Section IV-B we compare the experimentally measured buoy response to those expected from linear wave-current theory (Eq. (3)) to assess the importance of additional response functions to account for the modified dynamics.

III. Experimental set-up and methodology

A. Model design and manufacture

The experiments outlined here were all conducted with a spherical wave buoy of diameter 240 mm, under test in the FloWave facility as illustrated in Fig. 2. The experimental dataset was, in part, collected for validation and calibration of numerical modelling activities and the simplified plain spherical form was chosen to provide a more generic shape for this purpose. A challenging aspect of modelling a wave buoy experimentally is achieving representative geometric scaling in facilities where scales of approximately 1/10 - 1/20 are the norm. An earlier phase of experiments established that 6 degree-of-freedom (dof) data could not be reliably obtained from a smaller geometrically scaled buoy. The priority for this model was therefore to provide a reliable platform for obtaining this 6 dof data to feed into the modelling tasks without being constrained by meeting any specific scale. This larger-scale buoy was also found to have benefits when assessing vortex-induced motions as the vibrational 'regimes' will be more similar to those experienced at full-scale. Considering the depth of FloWave, the buoy diameter (approx. 0.3 m to 12 m full-scale), and the conditions tested (Section III-C) the representative scale for the experiments could be considered to be between 1:5 to 1:20 dependent on the buoy and the site location.

The model wave buoy was 3D printed in ABS and waterproofed with an epoxy sealant. The internal space could be accessed through a removable top cover for ballasting purposes, with the centre of gravity 40 mm below the mean water level (Fig. 2). A motion capture "tree" with four reflective markers was affixed to the top cover to provide 6 dof motion data, with origin set to the centre of the spherical body.

The model was deployed with both taut and elastic moorings. The taut mooring was constructed of 2 mm diameter Dyneema rope and was assumed to be infinitely stiff for the purposes of this experiment. The length was set to obtain a 30° angle with the vertical when taut (in 2 m water depth). The flexible mooring used 2 mm diameter elastic with a length of 1.7 m when unstretched. The elastic mooring stiffness (k_m) was measured as 6.73 ± 0.3 N/m.

B. Experimental set-up

The experimental programme was undertaken at the FloWave Ocean Energy Research Facility at The University of Edinburgh, UK (circular wave and current tank with a diameter of 25 m and a water depth of 2 m for the upper tank). The model was installed 1.64 m (streamwise) and 0.55 m (cross-tank) from tank centre in order to take advantage of the facility's AMTI OR6-7 floor mounted 6 dof force plate. The force plate was used to measure mooring loads under current, and all instrument locations and motions are referenced from this mooring anchor point, as illustrated in Fig. 3. The 6 dof motion of the buoy was captured based on the Qualisys motion capturing system.

Force plate data (under current only tests) and 6 dof motion data were collected. Additional open tank testing was conducted to characterise the sea states for both wave and current with the wave buoy removed. The tests used twin wire resistance wave gauges and a Nortek Vectrino2 ADV (acoustic doppler velocimeter) measuring at 0.2 m below the still water surface. The locations of these instruments, as per the coordinate system in Fig. 3, are described in Table I. The wave gauge array was placed over the model deployment location and the array designed to allow unidirectional reflection analysis (WG 1-5) with additional gauges for directional wave analysis.

C. Test plan

Experiments were carried out primarily to characterise the buoy response in simplified wave, current and combined wave-current conditions. These tests conditions are summarised in Table II. Tests were initially carried out with different current velocities

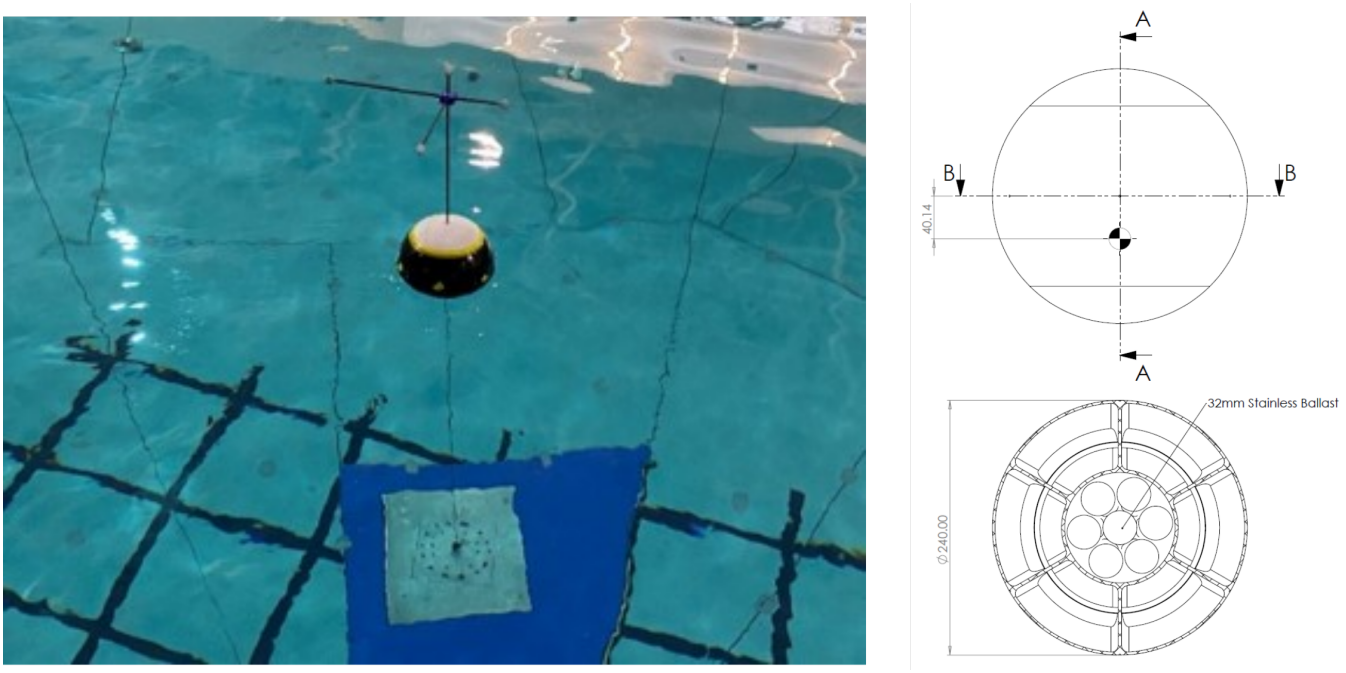

Fig. 2. Test installation schematic with origin and axis system for motion capture measurements and instrumentation locations. All dimensions mm.

TABLE I
INSTRUMENTATION LOCATIONS RELATIVE TO MOORING

	WG1	WG2	WG3	WG4	WG5	WG6	WG7	WG8	WG9	ADV
x [m]	0.909	0.727	0.273	0.000	-0.091	0.273	0.273	0.273	1.209	0
y [m]	0.000	0.000	0.000	0.000	0.000	-0.273	0.273	1.337	0.000	1.065

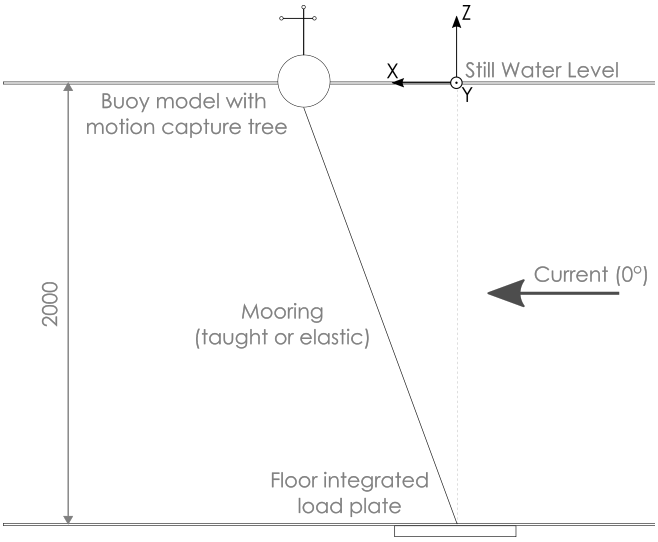

Fig. 3. Test installation schematic with origin and axis system for motion capture measurements and instrumentation locations. All dimensions in mm.

using both the taut and flexible mooring lines to assess the mean positions and response in current (current-only). Tests of varying wave frequency f (0.2 to 0.7 Hz) and a fixed input amplitude a_{in} of 0.03 m were also carried out in the absence of a current (wave-only). Subsequently, combined wave-current tests were carried out for the same f and a_{in} values both following and opposing a $\bar{U}$ = 0.2 m/s current. Lastly, a set of oblique tests were carried out with a fixed f of 0.4 Hz and a range of relative angles to a $\bar{U}$ = 0.2 m/s current. For all cases with waves only the flexible mooring line was used.

In addition to the characterisation tests, a series of tests were carried out with a directionally spread irregular sea state in a range of current speeds and relative angles (to the mean wave direction). The frequency spectrum was defined using a JONSWAP spectrum [10] with a significant wave height, H_{m0}, of 0.1 m, a peak period, T_p, of 2.5 s and a peak enhancement factor, γ, of 1. This low γ value ensures the spectrum is broad-banded to assess a wide frequency response. The directional spreading was defined using the Mitsuyasu model [11] (cos-2s) formulation with the spreading parameter, s, set to 5. This ensures the spectrum is also broad-banded in direction. The directionally-spread test conditions are summarised in Table III, noting that they were all carried out with the flexible mooring.

D. Test dataset

The test data, including 6 dof wave buoy motions; current induced mooring loads; wave gauge measurements; and ADV velocity data is freely available to download through The University of Edinburgh's Datashare service (https://doi.org/10.7488/ds/3105). Also available in this dataset is the detailed test log and 3D model of the wave buoy.

TABLE II
WAVE BUOY CHARACTERISATION TEST CONDITIONS

Type	Current	Waves	Mooring
Current-only	$\bar{U}$ = [0:0.05:0.45] m/s		taut, flexible
Wave-only		a_{in} = 0.03 m, f = [0.2:0.05:0.7] Hz, ζ = 0°	flexible
Following	$\bar{U}$ = 0.2 m/s	a_{in} = 0.03 m, f = [0.2:0.05:0.7] Hz, ζ = 0°	flexible
Opposing	$\bar{U}$ = 0.2 m/s	a_{in} = 0.03 m, f = [0.2:0.05:0.7] Hz, ζ = 180°	flexible
Oblique	$\bar{U}$ = 0.2 m/s	a_{in} = 0.03 m, f = 0.4 Hz, ζ = [0:22.5:180]°	flexible

TABLE III
DIRECTIONALLY-SPREAD TEST CONDITIONS

Type	Current	Waves
Following	$\bar{U}$ = [0:0.05:0.25] m/s	$H_{m0,in}$ = 0.1 m, T_p = 2.5 s, ζ = 0°
Opposing	$\bar{U}$ = [0:0.05:0.25] m/s	$H_{m0,in}$ = 0.1 m, T_p = 2.5 s, ζ = 180°
Oblique	$\bar{U}$ = [0.1, 0.2] m/s	$H_{m0,in}$ = 0.1 m, T_p = 2.5 s, ζ = [0:30:180]°

IV. RESULTS

A. Current-only conditions

The current-only tests were carried out primarily to assess the buoys mean positions in x and z (current along x-axis). This enables calculation of the current-modified draught and mooring line angle, determining the restoring forces in the z, x and y directions. Significant vortex-induced motions (VIM) were, however, noted during the experiments, resulting in large y – and to a lesser degree – x-motions which have the potential to affect the wave measurement performance.

The mean x and z positions, along with the force in the x-direction, F_x, are presented in Fig. 4 for both the taut and flexible mooring lines as a function of current speed. Standard deviations are represented by error bars. Compared to the taut mooring, the flexible line allows for significantly greater movement in the x-direction. This consequently results in a smaller reduction in z due to the reduced component of the line-tension in the vertical direction (compensated by increased buoyancy). F_x values are found to be comparable for both mooring lines as this is determined by the drag force. Slightly larger values of F_x are, however, noted for the flexible line, which is suspected to be a result of spatial variability of the current field in x, and the significantly different mean x positions of the buoy observed with the two mooring lines. In Fig. 4, the jump in Δx for the taut mooring line between $\bar{U} = 0$ m/s and $\bar{U} \approx 0.025$ m/s is a result of the length of the mooring line exceeding the water depth and being slack for 0 m/s.

The error bars in Fig. 4 demonstrate that there is significant variability in the position of the buoy (x and z) during the experiments. However, the majority of the motions in current-only conditions are in the y-direction and result from VIM. This is evident in Fig. 5, whereby x-y trajectories of the buoy in $\bar{U}$ = 0.25 m/s for both mooring lines are presented. For both moorings, there is a bias towards y-motions due to the VIM, and y-motions larger than the buoy diameter are observed. The trajectories themselves, however, differ greatly between the taut and stiff moorings. The motions for the taut mooring form an arc determined by the mooring length, whereas the flexible mooring motions are more chaotic and span a greater range of $x - y$ combinations.

To assess the VIM for all current speeds, the standard deviations of the motions in x, y and z are presented in Fig. 6 for both moorings. It is evident that the y-motions are dominant for both moorings. Assessing Fig. 6b, peak standard deviations – suggesting resonant behaviour – are observed in the region 0.2 m/s-0.3 m/s for both the taut and flexible lines. VIM for the taut mooring is observed to be larger and at significantly lower frequency (indicated by the marker shade), highlighting the effect of the mooring stiffness and configuration on the resulting buoy response. Larger z motions are also observed for the taut line due to the inability to respond to variations in x-forcing (e.g. turbulence) without a corresponding change to the z position. Section IV-B assesses the modified buoy response to waves in the presence of current, including the potential influence of VIM on the sampling of the wave field.

B. Regular waves and currents

Example outputs of the recorded buoy motions in the presence of regular waves and currents are presented in Figs. 7 and 8. As mentioned, only the flexible mooring line was installed for experiments with waves. Fig. 7 presents an opposing wave condition ($\theta = \zeta$ = 180°) where the y-motions are solely due to VIM, whilst Fig. 8 presents an oblique case where $\theta = \zeta$ = 45°. For both cases the z-motions are found to agree very well with the surface elevations measured using a wave gauge. The y-motions indicate the presence of large VIM as expected from Section IV-A, but at a significantly lower frequency than the waves. The x-motions also have a low frequency drift corresponding to the vortex-induced x-motions observed.

For the ζ = 45° cases presented in Fig. 8 the wave-induced x and y motions will be of equal amplitude, yet is evident that in the y-direction the VIM is significantly larger than the wave-induced motions. As VIM

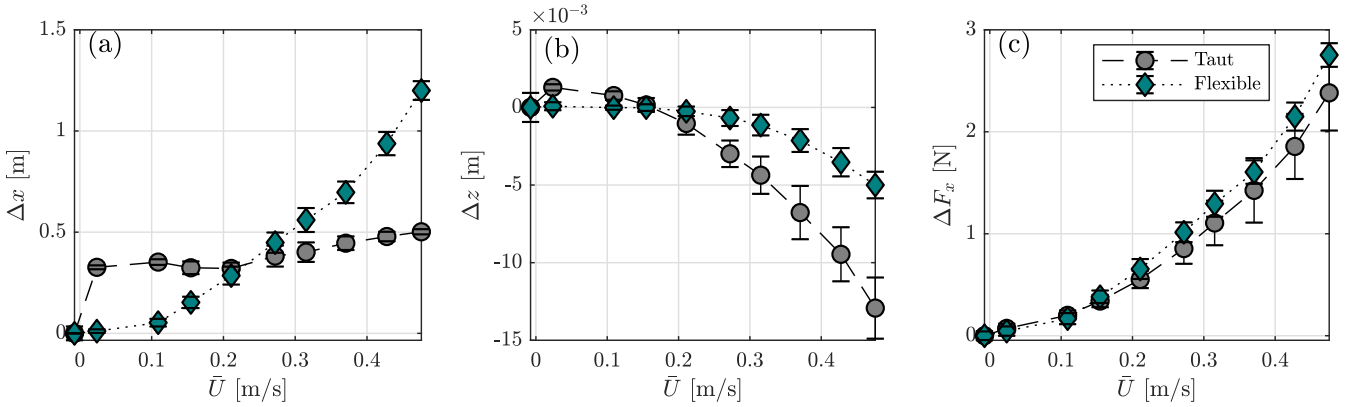

Fig. 4. Mean positions and forces for the buoy attached to taut and flexible mooring lines. a) mean change in x position as a function of current speed, b) mean change in z position as a function of current speed, c) mean change in F_x as a function of current speed. Standard deviations are represented by errorbars.

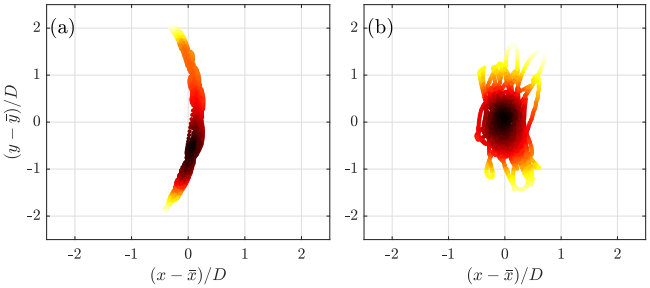

Fig. 5. Buoy trajectories for taut and flexible mooring lines in $\bar{U}$ = 0.25 m/s where the mean current direction is from left to right in the figure. a) trajectories for taut mooring line, b) trajectories for flexible mooring line. Colour is proportional to the probability density (black = high probability, yellow = low probability).

is not associated with a corresponding heave response, the VIM will only affect the interpretation of the wave climate if it alters the response at the wave frequencies (where there is a heave response). For these experiments, the significantly lower-frequency VIM should preclude any consistent effect on the motions observed at the wave frequencies.

To assess this response at the wave frequencies for all regular wave tests, the wave-induced vertical and horizontal motion amplitudes are extracted from Fast Fourier Transforms (FFTs) and are presented in Fig. 9. These values are compared to the theoretical values from Eq. (3), accounting for the current-modified wavenumbers. In Fig. 9 the total wave-induced horizontal response, $A_{x,y}$, is presented which is defined as:

$$A_{x,y} = \sqrt{A_x^2 + A_y^2} \tag{4}$$

where A_x and A_y are the FFT-isolated motion amplitudes at the wave frequency in the x and y directions respectively. A_z is also presented in Fig. 9 which corresponds to the vertical motion amplitudes (heave response).

Assessing first the heave response presented in Fig. 9. It is evident for all conditions presented there is good agreement between the measured heave and the amplitudes extracted from wave gauge measurements (no transfer function applied to buoy heave data, H_1 = 1). The potential exception is the high frequency opposing conditions (0.6–0.7 Hz) where larger heave response is measured than expected from wave gauge measurements. This is not expected to be a VIM-effect due to the large difference in frequencies. As this is not observed at the same observation frequency for the following and no-current conditions, it is concluded to be a dynamic response at the wavenumbers associated with these observation frequencies in the presence of opposing current. This may be a result of the higher wavenumbers and steepness for these conditions which could result in non-linear hydrodynamic forcing of the buoy. Increasing the steepness further could potentially increase the non-linear response and deviation from the predicted values.

The horizontal (surge) motions indicate a greater deviation from the expected linear wave theory particle trajectories. Large low frequency (0.2–0.25 Hz) amplitudes are observed for the no-current, following and opposing cases; suggesting this is a resonant mooring response. For the no-current and following cases, this is the only major discrepancy from theory. However, for the opposing cases, larger surge motions than predicted are observed for all frequencies. This suggests that for opposing conditions (higher k values), the dynamic response is significantly altered. This may be a result of the higher particle accelerations associated with these conditions – potentially coupled with the modified mooring dynamics and buoy draught due to current.

Assessing the oblique cases, the only notable discrepancy from linear theory occurs when the waves are opposing or 'near-opposing' the current, where the horizontal motions exceed the predicted values as observed for all opposing conditions. Wave amplitudes measured from the wave gauge and the buoy (A_z) are shown to increase with relative angle ζ – opposing condition amplitudes are close to double the following condition amplitudes. As the input amplitudes are the same for all relative angles, this highlights the extent of the wave-current interaction even for these relatively low current speeds.

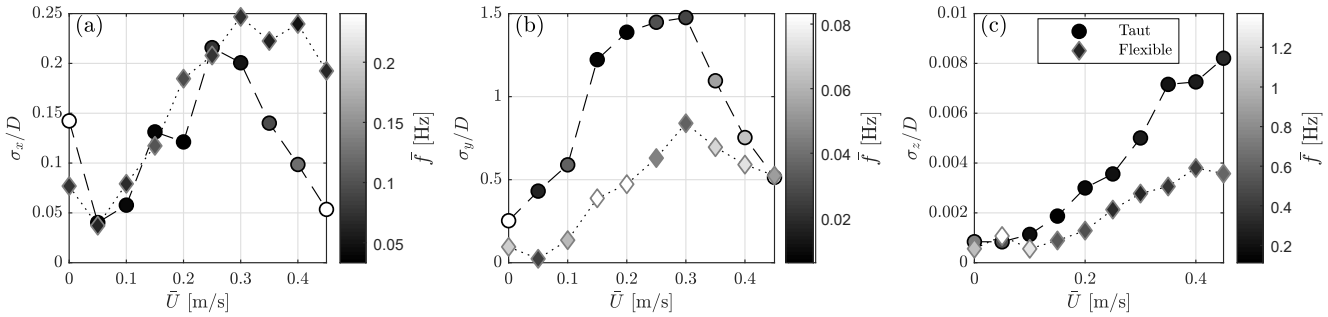

Fig. 6. Standard deviations of motions in x (left), y (centre) and z (right) as a function of mean current speed for current-only tests (Table II). Shown for both taut and flexible moorings. The shade of the markers indicate the mean frequency of the oscillations along the presented axes.

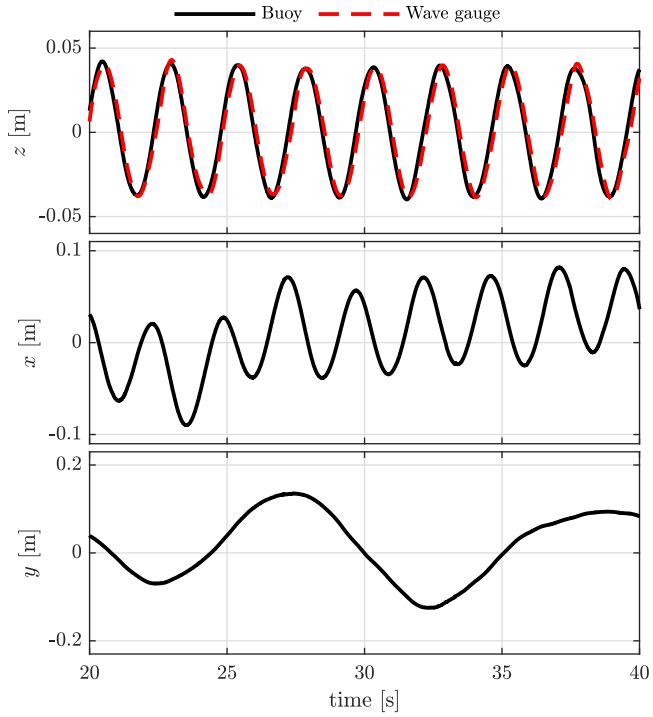

Fig. 7. Example buoy motions for an opposing wave condition: $\bar{U}$ = 0.2 m/s, f = 0.4 Hz, $\theta = \zeta$ = 180°

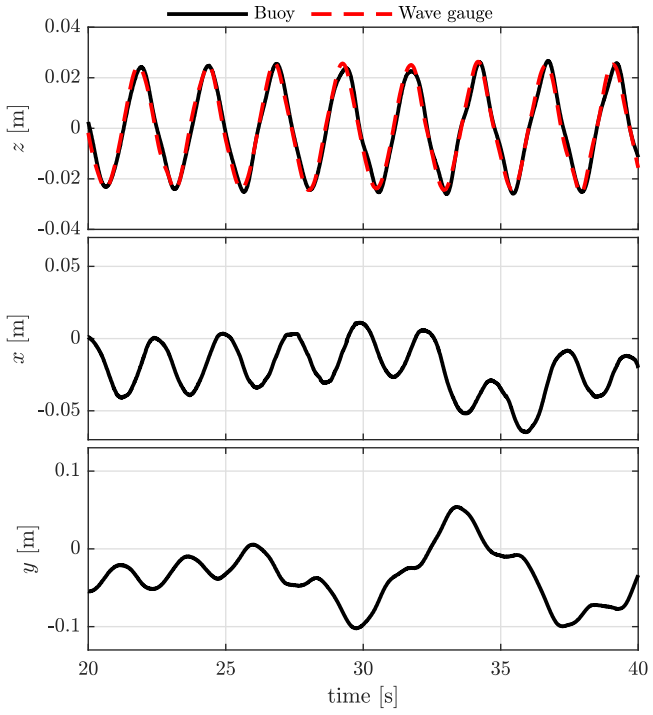

Fig. 8. Example buoy motions for an oblique wave condition: $\bar{U}$ = 0.2 m/s, f = 0.4 Hz, $\theta = \zeta$ = 45°

C. Directionally spread irregular waves in currents

The directionally spread irregular tests were primarily carried out to validate the analysis framework presented in [7], which is not the focus of this paper. However, an example output is presented here to demonstrate the buoys response in a realistic sea state with current over a wide range of frequencies. In Fig. 10, spectral outputs are presented for one of the opposing conditions in 0.15 m/s (see Table III). Both frequency and directional spectra are shown, where the Maximum Entropy Principle (MEP) is implemented to estimate the directional spectrum from the buoy measurements using Newton's method of local linearization [12]. Note that the standard assumption that wavenumber can be calculated using the dispersion relation without current is implemented.

Assessing Fig. 10a it is evident that there is good agreement between the frequency spectra measured with the buoy and the wave gauge. The associated H_{m0} values are also in agreement: a value of 0.1095 m was measured with the wave gauge and 0.1088 m measured with the buoy (0.6% discrepancy). The overprediction of the surface elevation at high frequencies observed in Fig. 9 is not apparent in the frequency spectrum comparison, which suggests that the result observed with regular waves may be due to nonlinear forcing due to the steepness of the conditions. Further exploration, with the use of a hydrodynamic model, is required to conclude on this.

In Fig. 10c the directional spectrum reconstructed from buoy measurements using the MEP approach is presented, which appears to correlate well to the input directional spreading (Fig. 10b). This suggests that despite the errors in the MEP approach implemented (incorrect wavenumbers assumed in transfer functions), the spreading can still be well estimated; agreeing with predictions made in [7].

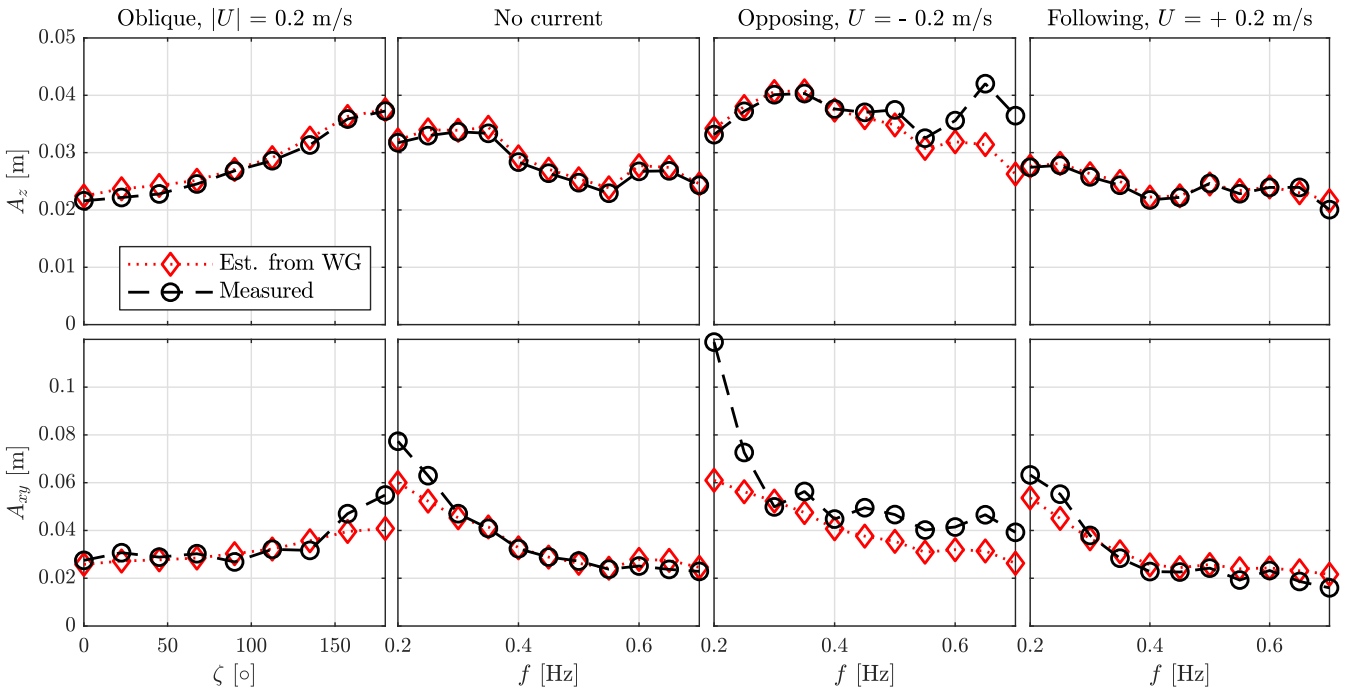

Fig. 9. Measured wave-induced vertical and horizontal motion amplitudes (black) compared to theoretical values from wave-current theory (red). (left) amplitudes as a function of relative angle, ζ, for 0.4 Hz waves in $\bar{U}$ = 0.2 m/s. (centre left) amplitudes as a function of frequency for wave-only conditions. (centre right) amplitudes as a function of frequency for opposing conditions in $\bar{U}$ = 0.2 m/s. (right) amplitudes as a function of frequency for following conditions in $\bar{U}$ = 0.2 m/s.

V. Discussion: Expanding Understanding to Full-Scale Buoys

A. Vortex-induced motions

In Section IV-A significant VIM was observed for the tank scale buoy. However, it was concluded in Section IV-B that due to the significant difference in frequency between the wave-induced motions and the VIM, that this will not have a consistent effect on the wave-induced response of the buoy (particularly when averaged over many cycles as in frequency-domain analysis). At full-scale, however, the spatial and temporal scales of the VIM relative to the wave-induced motions will be different. Firstly, the VIM frequency at full-scale (similar magnitude to experiments) is likely to be much closer to the full-scale wave frequencies and hence phase-locked effects may occur; resulting in a consistent offset in the measurements of some wave frequencies. However, the magnitudes of the VIM (similar magnitude to experiments) will be much smaller relative to the full-scale wavelengths and buoy motions, which will significantly diminish the effect on the sampling of the wave field. It is therefore expected that VIM at full-scale will not be a significant issue, however, the consequences of the mooring configuration and depth may affect these conclusions and a further assessment on full-scale data is warranted.

B. Wave-induced buoy response

Conclusions on the wave-induced buoy response in wave-current conditions presented in this paper are limited to tank-scale conditions with a simplified compliant mooring. Based on these preliminary observations it appears that the buoy response does not significantly deviate from the expected linear wave-current theory values other than (i) at low frequency due to mooring resonance/response, and (ii) for opposing conditions with high wavenumbers. If full-scale buoys behave similarly it may be sufficient to use linear wave-current theory transfer functions in place of buoy-specific transfer functions (Eq. (3), Fig. 9) when processing wave buoy data in the presence of currents. An assessment of the resulting errors and whether they are acceptable is still to be undertaken.

To robustly expand the understanding gained from the experiments, and assess the response of full-scale buoys with realistic moorings in full-scale conditions, future work will develop and validate a hydrodynamic model of the buoy against the presented experiments. After expanding the parameter space (e.g. geometry, mooring-configuration, wave-current conditions, depth) this will allow a robust assessment to be made on the requirement for buoy-mooring specific transfer functions, whilst providing a method to calculate these functions for inclusion in buoy processing methodologies (e.g. [7]).

C. Accounting for current in wave buoy measurements

The ultimate goal of the *Accounting for current in wave buoy measurements* project is to develop a reliable approach to process wave buoy data in the presence of current: correcting sea state parameters and estimating the current. The experiments presented in this paper will facilitate the development and validation of the methodology presented in [7] to achieve this.

Firstly, the characterisation tests (Table II, Sections IV-A and IV-B) give a preliminary understanding of the expected dynamic response in current and

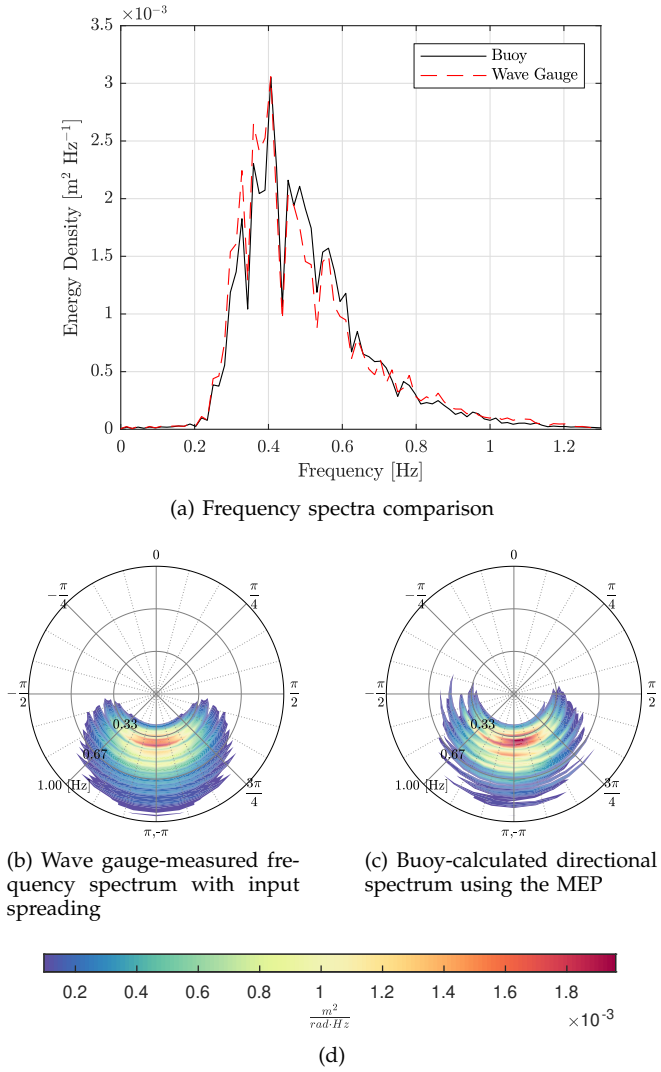

(a) Frequency spectra comparison

(b) Wave gauge-measured frequency spectrum with input spreading

(c) Buoy-calculated directional spectrum using the MEP

(d)

Fig. 10. Example outputs from the buoy in directionally spread irregular conditions in an opposing current of 0.15 m/s. Measured values of $H_{m0} = 0.1095$ m from the wave gauge and $H_{m0} = 0.1088$ m from the buoy.

provide a benchmark dataset for the validation of numerical models able to obtain transfer functions for full-scale buoys in real conditions. Secondly, the directionally-spread irregular tests in current (Table III, Section IV-C) provide a dataset which can be used to validate the overall buoy analysis framework presented in [7]. The inclusion of both buoy-specific, and generic transfer functions based on linear wave-current theory, can both be incorporated, and the methodology validated before being applied to full-scale datasets. Ultimately, it is envisaged this will lead to improved sea state parameters extracted from wave buoy data, increasing the accuracy and reliability of wide-area models and the design process for offshore renewable energy systems.

VI. Conclusion

To assess the effect of current on wave buoy measurements, we present experimental results obtained for a model-scale wave measurement buoy in the presence of a range of combined wave-current conditions. In current-only conditions, significant VIM are observed, the nature and magnitude of which are found to be highly sensitive to mooring stiffness and current speed. Resonant VIM is observed for both taut and flexible moorings in the region of 0.2 m/s where y motions are found to exceed the buoy diameter.

Assessing the buoy response in regular waves and currents, it is concluded that the aforementioned VIM does not affect the wave-induced response due to the significant difference in frequency observed between the VIM and wave-induced motions. VIM is subsequently concluded to be unlikely to significantly alter wave measurements at full-scale. The measured buoy motion amplitudes (horizontal and vertical) are found to agree with theoretical predictions based on linear wave-current theory other than (i) at low frequency due to mooring resonance, and (ii) for wave conditions opposing the current. For opposing conditions, surge motions are found to exceed linear predictions for all wave frequencies tested, and the surface elevation is found to be over-estimated for the high frequency (and steepness) waves. Results in directionally-spread irregular conditions, however, show no bias in the high-frequency heave response and the buoy is found to measure near-identical frequency spectra to a wire wave gauge.

The observations for regular wave-current conditions suggest that modified transfer functions may be required in the presence of current (particularly for wave components opposing the current) in order to accurately estimate the true underlying sea state parameters. Hydrodynamic models will be validated against this dataset (available at https://doi.org/10.7488/ds/3105) to increase understanding and expand to full-scale buoys of varied geometry and mooring configurations. The directionally-spread irregular test cases will be used to validate analysis methodologies (such as [7]) designed to account for, and estimate, the current and improve sea state parameters; knowledge of modified transfer functions will further improve performance. Improved sea state parameters extracted from wave buoy data will ultimately decrease uncertainty in the design process for offshore renewable energy systems.

Acknowledgement

The authors would like to thank Dr Laura-Beth Jordan and Martyn Lennon at the FloWave Ocean Energy Research Facility for their help in preparing and executing the experiments.

References

[1] M. J. Tucker and E. G. Pitt, *Waves in ocean engineering*, 2001, no. Volume 5.
[2] F. I. Gonzales, "A Case Study of Wave-Current-Bathymetry Interactions at Columbia River Entrance," *Journal of Physical Oceanography*, vol. 14, pp. 1065–1078, 1984.
[3] H. L. Tolman, "Effects of Tides and Storm Surges on North Sea Wind Waves," *Journal of Physical Oceanography*, vol. 21, pp. 766–781, 1990.
[4] D. W. Wang, A. K. Liu, Y. P. Chih, and E. A. Meindl, "Wave-current interaction near the Gulf Stream during the Surface Wave Dynamics Experiment," *Journal of Geophysical Research*, vol. 99, no. C3, pp. 5065–5079, 1994.
[5] C. Macisaac and S. Naeth, "TRIAXYS Next Wave II Directional Wave Sensor The Evolution of Wave Measurements," *2013 OCEANS - San Diego*, pp. 1–8, 2013.

[6] Y. Pérignon, J. Thomson, A. Benetazzo, P. Sutherland, P. Ferrant, P. Veras Guimarães, M. Accensi, F. Ardhuin, and M. Hamon, "A surface kinematics buoy (SKIB) for wave–current interaction studies," *Ocean Science*, vol. 14, no. 6, pp. 1449–1460, 2018.
[7] A. C. Pillai, T. Davey, and S. Draycott, "A framework for processing wave buoy measurements in the presence of current," *Applied Ocean Research*, vol. 106, p. 102420, 2021.
[8] D. Peregrine, "Interaction of Water Waves and Currents," in *Advances in Applied Mathematics*, ser. Advances in Applied Mechanics, C.-S. Yih, Ed. Elsevier, 1976, vol. 16, pp. 9–117. [Online]. Available: http://www.sciencedirect.com/science/article/pii/S0065215608700875
[9] M. Benoit, P. Frigaard, and H. A. Schaäffer, "Analysing Multidirectional Wave Spectra: a Tentative Classification of Available Methods," *Proceedings IAHR Seminar on Multidirectional Waves and their Interaction whith Structures*, pp. 131–154, 1997.
[10] K. Hasselmann *et al.*, "Measurements of wind-wave growth and swell decay during the joint North Sea wave project (JONSWAP)." Deutsches Hydrographisches Institut - Hamburg, Tech. Rep. January, 1973.
[11] H. Mitsuyasu, F. Tasai, T. Suhara, S. Mizuno, M. Ohkusu, T. Honda, and K. Rikiishi, "Observations of the directional spectrum of ocean wavesusing a cloverleaf buoy," *Journal of Physical Oceanography*, vol. 5, no. 4, pp. 750–760, 1975.
[12] N. Hashimoto, "Analysis of the directional wave spectrum from field data," in *Advances in coastal and ocean engineering*. World Scientific, 1997, pp. 103–143.